THE JOURNAL OF BIOLOGICAL CHEMISTRY
Vol. 280, No. 18, Issue of May 6, pp. 18063–18072, 2005
Printed in U.S.A.

Structural Studies of a Stabilized Phosphoenzyme Intermediate of Ca^{2+}-ATPase*

Received for publication, January 3, 2005, and in revised form, February 23, 2005
Published, JBC Papers in Press, February 25, 2005, DOI 10.1074/jbc.M500031200

David L. Stokes‡§¶, Franck Delavoie‖, William J. Rice‡, Philippe Champeil, David B. McIntosh‡‡§§, and Jean-Jacques Lacapère‖¶¶**

*From the ‡Skirball Institute of Biomolecular Medicine and Department of Cell Biology, New York University School of Medicine, New York, New York 10012, the §New York Structural Biology Center, New York, New York 10027, ‖U410 INSERM, Faculté de Medicine Xavier Bichat, 16 rue Henri Huchard, B.P. 416, 75870 Paris cedex 18, France, **URA CNRS 2096 and SBPM/DBCM, CEA Saclay, 91191 Gif-sur-Yvette cedex, France, and the ‡‡Institute of Infectious Diseases and Molecular Medicine, University of Cape Town, Observatory, Cape Town 7925, South Africa*

Ca^{2+}-ATPase belongs to the family of P-type ATPases and maintains low concentrations of intracellular Ca^{2+}. Its reaction cycle consists of four main intermediates that alternate ion binding in the transmembrane domain with phosphorylation of an aspartate residue in a cytoplasmic domain. Previous work characterized an ultrastable phosphoenzyme produced first by labeling with fluorescein isothiocyanate, then by allowing this labeled enzyme to establish a maximal Ca^{2+} gradient, and finally by removing Ca^{2+} from the solution. This phosphoenzyme is characterized by very low fluorescence and has specific enzymatic properties suggesting the existence of a high energy phosphoryl bond. To study the structural properties of this phosphoenzyme, we used cryoelectron microscopy of two-dimensional crystals formed in the presence of decavanadate and determined the structure at 8-Å resolution. To our surprise we found that at this resolution the low fluorescence phosphoenzyme had a structure similar to that of the native enzyme crystallized under equivalent conditions. We went on to use glutaraldehyde cross-linking and proteolysis for independent structural assessment and concluded that, like the unphosphorylated native enzyme, Ca^{2+} and vanadate exert a strong influence over the global structure of this low fluorescence phosphoenzyme. Based on a structural model with fluorescein isothiocyanate bound at the ATP site, we suggest that the stability as well as the low fluorescence of this phosphoenzyme is due to a fluorescein-mediated cross-link between two cytoplasmic domains that prevents hydrolysis of the aspartyl phosphate. Finally, we consider the alternative possibility that phosphate transfer to fluorescein itself could explain the properties of this low fluorescence species.

Intracellular Ca^{2+} concentrations are maintained at low levels by a group of ATP-dependent Ca^{2+} pumps that belong to the family of P-type ATPases (1, 2). These pumps maintain low intracellular Ca^{2+} concentrations as a baseline for signal transduction pathways initiated by opening a variety of Ca^{2+} channels. There are distinct groups of Ca^{2+} pumps, or Ca^{2+}-ATPases, in the plasma membrane and in membranes of the sarcoplasmic/endoplasmic reticulum. The particular isoform from sarcoplasmic reticulum (SR)[1] of skeletal muscle is the most extensively studied and represents an archetype for the entire family. Biochemical studies have defined a series of reaction intermediates that couple the energy of ATP hydrolysis within the cytoplasmic domain to alternations in the affinity and accessibility of Ca^{2+} binding sites within the membrane domain (3). In the key step of the reaction cycle, this energy is stored by the pump as an aspartyl phosphate and is used to drive a global conformational change that simultaneously lowers the affinity of the Ca^{2+} sites and exposes them to the luminal side of the membrane, where the Ca^{2+} ions are exchanged with protons. In fact, the reaction cycle appears to be driven by a series of such conformational changes, which have been deduced by biochemical and spectroscopic means and, in some cases, directly visualized by electron microscopy (EM) and x-ray crystallography (4, 5).

In its simplest form, this reaction cycle consists of four intermediates that alternate steps of ion binding/release with those of phosphorylation/dephosphorylation of an aspartate residue. This aspartate resides at the heart of the catalytic site, and its phosphorylation by ATP is a critical step in transducing chemical energy into conformational energy for Ca^{2+} transport. As outlined in Scheme 1, binding of cytoplasmic Ca^{2+} is followed by formation of a "high energy" phosphoenzyme, commonly denoted either $E\sim P[Ca_2]$ or $E_1\sim P[Ca_2]$, in which two Ca^{2+} ions become "occluded" within the transmembrane domain, as denoted by brackets: $[Ca_2]$. A global conformational change to a low energy phosphoenzyme (E-P or E_2-P) exposes the Ca^{2+} sites to the luminal side of the membrane and lowers their affinity to the millimolar range; after Ca^{2+} release and proton binding, the phosphoenzyme is hydrolyzed to complete the cycle. E_1 and E_2 are frequently used to distinguish two hypothetical conformational states of the enzyme. E_1 exists in the first half of the cycle with high affinity Ca^{2+} sites either cytoplasmically oriented or occluded and the catalytic aspar-

* This work was supported in part by National Institutes of Health Grant R01-GM56960 (to D. L. S.) and Human Frontier Science Program Grant RGP0060/200-M (to P. C.). The costs of publication of this article were defrayed in part by the payment of page charges. This article must therefore be hereby marked "*advertisement*" in accordance with 18 U.S.C. Section 1734 solely to indicate this fact.

¶ To whom correspondence may be addressed: Skirball Institute of Biomolecular Medicine, NY University School of Medicine, 540 First Ave., New York, NY 10012. Tel.: 212-263-1580; Fax: 646-219-0300; E-mail: stokes@saturn.med.nyu.edu.

§§ Supported by the University of Cape Town Research Committee, National Research Foundation of South Africa, and National Health Laboratory Service of South Africa.

¶¶ To whom correspondence may be addressed: U410 INSERM, Faculté de Medicine Xavier Bichat,16 rue Henri Huchard, B.P. 416, 75870 Paris cedex 18, France. Tel.: 33-1-4485-6136; Fax: 33-1-4228-8765; E-mail: Jean-Jacques.Lacapere@bichat.inserm.fr.

[1] The abbreviations used are: SR, sarcoplasmic reticulum; EM, electron microscopy; TG, thapsigargin; FITC, fluorescein isothiocyanate; AcP, acetyl phosphate; PK, proteinase K; EPPS, 4-(2-hydroxyethyl)-1-piperazinepropanesulfonic acid;

tate reactive toward nucleotides. E_2 exists in the second half of the cycle with the aspartate reactive toward inorganic phosphate and low affinity Ca^{2+} sites either exposed to the lumen or occluded with bound protons. Although the E_1/E_2 dichotomy has been shown by Jencks and others to be an oversimplification (6), it offers a framework for discussing the observed structural changes of the enzyme.

$$E_1 + 2Ca_{cyt} \rightarrow E_1(Ca_2) + ATP \rightarrow E_1{\sim}P[Ca_2] +$$

$$ADP \rightarrow E_2\text{-}P(Ca_2) \rightarrow E_2\text{-}P + 2Ca_{lum} \rightarrow E_2 + P_i$$

SCHEME 1

In recent years, the structures of four main intermediates have been defined by x-ray crystallography and electron microscopy (4, 5, 7). These structures have taught us a great deal about the conformational changes that drive the reaction cycle and about how binding of particular substrates dictates the domain interactions responsible for these conformational changes. Specifically, binding of Ca^{2+} to transport sites induces substantial changes to the backbone of several transmembrane helices; these changes are relayed by M4 and M5 to the cytoplasmic domain containing the catalytic aspartate (P-domain), causing its inclination and thus altering its association with the other cytoplasmic domains (denoted N- and A-domains). As a result, the aspartate is accessible to ATP bound in the N-domain, and phosphate transfer produces a chemical bridge between these two domains that indirectly induces Ca^{2+} occlusion. Loss of ADP disrupts this bridge and allows conserved residues on the A-domain to interact with the covalently bound phosphate group in the P-domain, thus indirectly disrupting the Ca^{2+} sites and opening the luminal gate for Ca^{2+} release. These same residues also orient a water molecule for hydrolysis of the aspartyl phosphate, which loosens the interaction between cytoplasmic domains and leads to proton occlusion at the transport site.

Despite these tremendous insights into the mechanisms of energy coupling, questions remain about the transitions between these intermediates and about the precise physiological context of each individual structure. In particular, the crystals used for structure determination generally require surrogate substrates to lock Ca^{2+}-ATPase into a defined conformation, and crystal contacts have the potential to influence the juxtaposition of loosely bound domains. For instance, although crystallization of the Ca^{2+}-bound state ($E_1(Ca_2)$) simply requires high concentrations of Ca^{2+} (8), the crystal contacts are likely to be responsible in part for the wide spread between the N-domain and the A-domain observed in the corresponding structure. Also, the Ca^{2+}-free state (E_2) was stabilized with thapsigargin (TG) (9), which is documented to have significant effects on binding of physiological ligands like ATP (10) and phospholamban (11), and the high energy phosphoenzyme ($E_1{\sim}P$) was trapped with the transition state analogue AlF_4^- in the presence of ADP (12), thus representing an analog of the phosphoenzyme prior to nucleotide release ($E_1{\sim}P[Ca_2]{\cdot}ADP$). Finally, an analog of the low energy phosphoenzyme ($E_2{\sim}P$) was crystallized with the MgF_4^{2-} or the AlF_4^- ligand bound to the catalytic aspartate, again including TG (13, 14), which may again be expected to exert a non-physiological influence over the conformation. Similarly, lower resolution studies of the low energy phosphoenzyme employed decavanadate as a crystallization agent, which bound at the interface of the three cytoplasmic domains (15).

An alternative procedure has been described for stabilizing a phosphoenzyme derived from the high energy intermediate, and structural characterization of this phosphoenzyme therefore holds the potential to shed light on the occlusion of calcium and on other conformational changes of the phosphoenzyme (16). Formation of this stabilized phosphoenzyme requires covalent labeling of Ca^{2+}-ATPase with fluorescein isothiocyanate (FITC), which has long been known to be specific for Lys^{515} within the ATP binding site. Indeed, fluorescent changes of FITC have often been used to monitor conformational changes during the reaction cycle (17). Although FITC labeling prevents phosphorylation by ATP, acetyl phosphate (AcP) can be used to pump Ca^{2+} and to produce high levels of the phosphoenzyme once the membrane-bound enzyme becomes inhibited by high luminal Ca^{2+} concentration. Upon sudden chelation of Ca^{2+} from the cytoplasmic side of the membrane, the FITC-labeled Ca^{2+}-ATPase can then be markedly stabilized in a low fluorescence, phosphorylated form. Characterization of the resulting species showed that, although it lacked bound Ca^{2+} ions, it could rapidly re-bind cytoplasmic Ca^{2+} with high affinity and transport this Ca^{2+} directly across the membrane. This FITC-labeled, low fluorescence species can thus be safely assumed to derive from $E_1{\sim}P[Ca_2]$, or rather from the transient species formed immediately prior to Ca^{2+} occlusion ($E_1{\sim}P(Ca_2)$). The ability of decavanadate to produce two-dimensional crystals within these vesicles (18) offers an opportunity to study the structural properties of this phosphoenzyme and to relate it to the other structures mentioned above.

For the current study, we optimized conditions for generating long, tubular crystals of the FITC-labeled, low fluorescence phosphoenzyme, which included addition of TG and decavanadate (19, 20), and solved its structure at 8-Å resolution by cryoelectron microscopy and helical image analysis. Unexpectedly, the resulting structure appeared to be very similar at this resolution to that previously determined for the unlabeled, unphosphorylated enzyme under analogous conditions. We then used proteolytic cleavage and glutaraldehyde cross-linking to bring other approaches to bear on the structural analysis and to study the influence of the crystallizing conditions (namely decavanadate) on the conformation adopted by this phosphoenzyme. In the absence of decavanadate, we obtained conflicting results from proteolytic cleavage with trypsin and proteinase K (PK), suggestive of a hybrid conformation, whereas in the presence of decavanadate the results were consistent with an E_2-like conformation, as borne out by our cryoelectron microscopic structure. We conclude that, like in the unphosphorylated native enzyme, Ca^{2+} and vanadate exert a strong influence over the global structure of the low fluorescence phosphoenzyme. Also, although FITC is likely to mediate a cross-link between N- and P-domains that serves to protect the aspartyl phosphate, this cross-link is different than that formed by ATP during phosphate transfer. Finally, we consider the alternative possibility that FITC itself could have become phosphorylated.

MATERIALS AND METHODS

SR was prepared from the white muscle of rabbit as described by Inesi and Eletr (21) or by Champeil *et al.* (22). For most labeling experiments, the preparation was diluted to 2 mg/ml protein in a buffer containing 10 mM Tris-Tricine, pH 8, 0.3 M sucrose, 1 mM $MgCl_2$, 10 μM $CaCl_2$, and 16 μM FITC, and incubated at 20 °C. The loss in ATPase activity, measured using a coupled enzyme assay (23), was used to follow the time course of labeling, which was generally complete after 15 min. The stabilized, high energy phosphoenzyme was generated as previously described (18) in a buffer containing 0.1–0.5 mg/ml SR, 100 mM KCl, 5 mM $MgCl_2$, and 50 mM MOPS at pH 7 and 20 °C. During this process, FITC fluorescence was monitored with excitation and emission wavelengths of 495 and 517 nm, respectively.

^{32}P incorporation into Ca^{2+}-ATPase after reaction with [^{32}P]-acetylphosphate (synthesized according to Bodley *et al.* (24)) was determined by acid precipitation and filtration on Whatman filters followed by washing with cold buffer and scintillation counting. Alternatively, for monitoring the long term stability of this phosphoenzyme, samples

were applied to a PD10 column pre-equilibrated with cold buffer to remove excess of radioactivity; collected fractions were centrifuged at 70,000 × *g* for 30 min in a Beckman rotor TLA 100.3, and the resultant pellet was resuspended in crystallization buffer prior to incubation for various periods and determination of the residual phosphorylation by filtration and scintillation counting.

Tryptic cleavage was carried out at 0.75 or 2 mg/ml SR and at a trypsin:SR weight ratio of 1:50 and was stopped by acid precipitation using 4% perchloric acid. Samples were then loaded onto 12% Laemmli gels for SDS-PAGE and stained with Coomassie Blue. Proteinase K cleavage was carried out at 2 mg/ml SR and with a PK/SR weight ratio of 1:67. SDS-PAGE after proteolysis arrest was performed as previously described (25).

For the glutaraldehyde cross-linking experiments, SR vesicles (4 mg/ml) were labeled with FITC in 50 mM EPPS/tetramethylammonium hydroxide, pH 8.0, 0.3 M sucrose, 0.1 mM $CaCl_2$, 2 mM $MgCl_2$, and 8 nmol/mg FITC for 20 min at room temperature. The suspension was then adjusted to pH 7.5 with a small aliquot of concentrated maleic acid and placed on ice. Formation of the low fluorescence species was performed at room temperature in 50 mM MOPS/tetramethylammonium hydroxide, pH 7.5, 0.3 M sucrose, 2 mM $MgCl_2$, 0.1 mM $CaCl_2$, 100 mM NaCl, 2 mM AcP, and 0.4 mg/ml SR protein labeled with FITC; unlabeled vesicles were also incubated as a control. Ca^{2+} loading was continued for 2 min, followed by addition of 5 mM EGTA to induce the low fluorescence species. Cross-linking was performed with 1 mM glutaraldehyde over 4 min in the same basic medium of 50 mM MOPS/tetramethylammonium hydroxide, pH 7.5, 0.3 M sucrose, 2 mM $MgCl_2$, and 100 mM NaCl with various additions as indicated in the legend to Fig. 4. The reaction was stopped by the addition of 1/10 dilution of 20% SDS, 5.4 M 2-mercaptoethanol, and a trace of bromphenol blue. The solubilized samples were subjected to SDS-PAGE with 7.5% acrylamide, and the proteins were stained with Coomassie Blue.

For preparing tubular crystals, FITC-labeled SR vesicles at 0.5 mg/ml protein were treated with 10 mM AcP, 5 mM $MgCl_2$, and 0.1 mM $CaCl_2$ at room temperature, and the phosphoenzyme formed was then stabilized by adding 5 mM EGTA followed by 10 μM TG. The fluorescence signal from FITC was used to monitor the formation of the low fluorescence species. Aliquots of 1 ml were then centrifuged at 70,000 × *g* for 30 min as above. After removing the supernatant, crystallization buffer (typically 100 μl) containing 20 mM imidazole, pH 7.2, 100 mM KCl, 5 mM $MgCl_2$, and 0.5 mM decavanadate was gently added to the pellet without resuspension, followed by three cycles of freezing and thawing to induce fusion of individual SR vesicles, thus producing larger tubular crystals (20). Protein concentrations above 10 mg/ml were required for significant fusion, with optimal results coming from the much higher concentration within a gelatinous pellet. Also, sucrose proved to be a strong inhibitor of fusion, and samples were therefore washed thoroughly prior to crystallization. After freeze-thaw, the pellet was resuspended at 1 mg/ml and incubated on ice overnight. For imaging, 5 μl of this sample was pipetted onto a perforated carbon film, blotted with filter paper, and quick frozen with liquid ethane. Low dose images were recorded at a magnification of ×50,000 and defocus of 0.8–1.8 μm with a CM200FEG electron microscope (FEI Corp., Eindhoven, Netherlands), screened by optical diffraction, and digitized at 14-μm intervals with a SCAI densitometer (Intergraph Corp., Madison, AL). After selecting well ordered tubes by optical diffraction, a group with a common helical symmetry (characterized by Bessel orders of −23 and 7 for the 1,0 and 0,1 layer lines, respectively) was selected for further processing. Defocus values were determined directly from the images (26), and, after applying 2-fold symmetry averaging, an initial three-dimensional structure was created using standard methods of helical reconstruction. This structure was used as a reference for a suite of programs designed to account for distortions along the tubes (27). Thereafter, a new reference was generated and the distortions were refined by a single iteration of these programs (15). Defocus values were used to correct phases and to weight amplitudes along the layer lines. These weighted data were then averaged and fully compensated for defocus effects. The final data set was filtered, by removing data points with phase deviations >65° from those expected for crystallographic 2-fold symmetry and was truncated at 7-Å resolution. This final structure was aligned with that of the unlabeled, unphosphorylated enzyme by selecting a single molecule from the crystal lattice with a Gaussian mask and then using the program suite Spider (28).

RESULTS

Formation and Characterization of the FITC-labeled, Low Fluorescence Phosphoenzyme—Early work revealed the formation under specific conditions of a species of FITC-labeled Ca^{2+}-ATPase with very low fluorescence (29), and, more recently, this species was shown by kinetic analysis to derive from the high energy phosphoenzyme after dissociation of the Ca^{2+} ions toward the cytosol (16). Fig. 1*A* shows a typical preparation in which the fluorescence initially falls slowly as phosphoenzyme is formed during active loading of SR vesicles with AcP. Upon addition of EGTA, there is a further, precipitous reduction in fluorescence by ~60% to a state that is stabilized by TG. Fig. 1*B* shows that, if TG is added prior to EGTA, this low fluorescence species is not formed; similarly, collapse of the Ca^{2+} gradient with Ca^{2+} ionophore (A23187) reverses the initial fluorescence decrease induced by AcP or prevents it from forming if added prior to AcP (not shown). Fig. 1*A* also shows that the low fluorescence state is maintained after subsequent addition of decavanadate (18). The fact that decavanadate actually binds to this species is documented by the slight decrease in fluorescence caused by decavanadate addition. This decrease is comparable, in relative terms, to that seen when decavanadate is added to the high fluorescence species (not shown, but see Ref. 30), and is not simply due to absorption of the excitation wavelength by decavanadate.

We used [^{32}P]AcP to quantify the amount of covalent phosphoenzyme formed under various conditions. During active loading of SR vesicles with [^{32}P]AcP, phosphoenzyme formation was complete after 4 min, reaching a maximal value of >7 nmol of phosphoenzyme/mg of protein (*black circles*, Fig. 1*C*). In the presence of Ca^{2+} ionophore A23187, the maximal level of phosphoenzyme was only 2 nmol/mg of protein (*gray triangles*), and measurements in the absence of Ca^{2+} (*gray squares*) demonstrated the baseline for these measurements. Thus, the presence of a Ca^{2+} gradient is a prerequisite for maximal phosphorylation of FITC-labeled ATPase by AcP. Furthermore, the levels reached by active loading with AcP are close to stoichiometric with the expected amount of FITC-labeled Ca^{2+}-ATPase, and somewhat higher than those obtained with vesicles preloaded with Ca^{2+} and phosphorylated from [^{32}P]P_i (16, 18).

Fig. 1*C* also shows that when EGTA was followed by TG, phosphoenzyme levels were completely stable over a 10-min period (*open circles*), similar to previous results with Ca^{2+}-preloaded vesicles phosphorylated from [^{32}P]P_i (18). On the other hand, when TG was added to the phosphoenzyme prior to EGTA, thus preventing formation of the low fluorescence state (Fig. 1*B*), the phosphoenzyme decayed with a half-life of 1–2 min (Fig. 1*C*, *open triangles*). A similar decay was observed when Ca^{2+} ionophore A23187 was added after phosphorylation (Fig. 1*C*, *open squares*). A comparison of fluorescence levels (Fig. 1, *A* and *B*) with phosphoenzyme levels (Fig. 1*C*) reveals that the intermediate fluorescence species induced by AcP loading, and the low fluorescence species induced by subsequent addition of EGTA, both correspond to maximal levels of phosphoenzyme. Based on the fact that bound Ca^{2+} could dissociate from it, the intermediate fluorescence species has been hypothesized to correspond to the normally transient enzymatic state occurring immediately prior to occlusion of Ca^{2+} (E_1~P(Ca_2)), perhaps in rapid equilibrium with the generally more stable occluded state (E_1~P[Ca_2]). The EGTA-induced decrease in fluorescence reflects the removal of Ca^{2+} from the former species (16).

To test the stability of this phosphoenzyme under conditions and time scales suitable for crystallization, we monitored ^{32}P retention by the FITC-labeled Ca^{2+}-ATPase upon incubation for days at 0 °C in a crystallization buffer containing EGTA, TG, and decavanadate. Fig. 1*D* shows that the level of phosphoenzyme, initially formed by active loading with AcP fol-

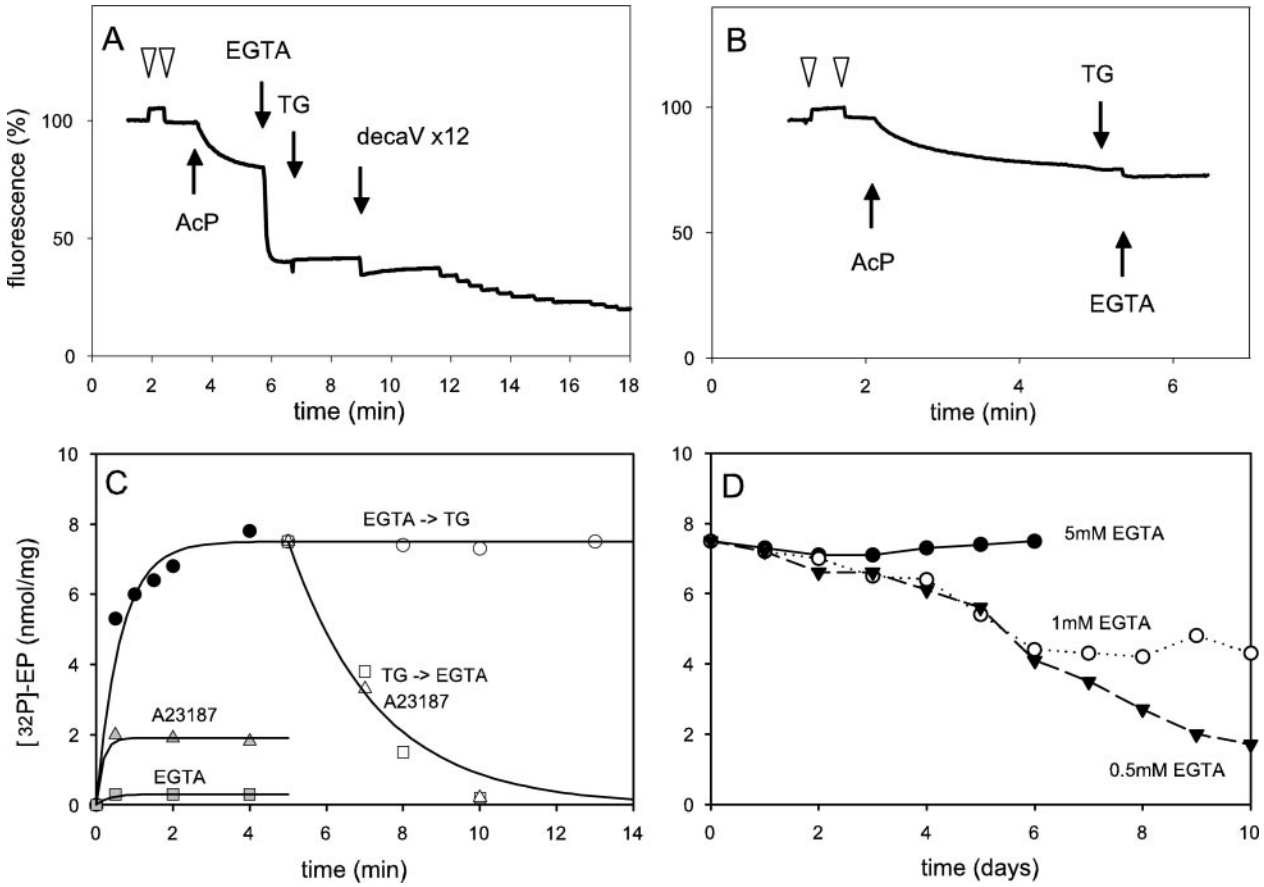

FIG. 1. **Formation of a low fluorescence phosphoenzyme from FITC-ATPase using AcP.** For the fluorescence studies (*A* and *B*), FITC-labeled SR vesicles were suspended at 0.1 mg/ml in 2 ml of buffer consisting of 50 mM MOPS-KOH at pH 7.0, 100 mM KCl, and 5 mM $MgCl_2$. For each trace, 90 μM EGTA was first added, followed by 100 μM Ca^{2+} (*open arrowheads*), thus producing the small, but well known Ca^{2+}-dependent FITC fluorescence changes as a calibration. Thereafter, phosphorylation was initiated by adding 10 mM AcP. *A*, after allowing the system to reach AcP-dependent steady-state fluorescence, the low fluorescence species (to be studied by electron microscopy) was generated by adding 2 mM EGTA, followed by 10 μM TG. Subsequent addition of decavanadate did not affect the stability of the low fluorescence form, although it further reduced its fluorescence slightly. *B*, the low fluorescence species is not formed if 10 μM TG is added prior to 2 mM EGTA. [^{32}P]AcP was then used to document the formation and stability of the low fluorescence phosphoenzyme. *C*, FITC-labeled SR vesicles (1 mg/ml) were incubated either in the presence (*black circles*) or in the absence (*gray squares*) of Ca^{2+}, or in the presence of Ca^{2+} together with the Ca^{2+} ionophore A23187 (*gray triangles*), prior to the addition of 10 mM of [^{32}P]AcP at time zero. After 5 min, samples in the presence of Ca^{2+} were subjected to sequential additions of 5 mM EGTA followed by 10 μM TG (*open circles*), of TG followed by EGTA (*open squares*), or of 5% (w/w) A23197 (*open triangles*). *D*, long term stability of the phosphoenzyme formed as shown in *A* and *C* and incubated in crystallization buffer was measured in 5 mM (*solid circles*), 1 mM (*open circles*), or 0.5 mM (*inverted triangles*) EGTA. Unreacted [^{32}P]AcP was eliminated using a PD10 column pre-equilibrated in AcP-free phosphorylation buffer. The collected fractions were centrifuged (40,000 rpm in a TLA 100.3 rotor for 30 min), and the pellet was resuspended at a protein concentration of 30 mg/ml in 50 mM MOPS-KOH, pH 7.0, 5 mM $MgCl_2$ and the stated concentrations of EGTA. After several cycles of freeze-thaw, the protein was diluted to 3 mg/ml in crystallization buffer, including TG and decavanadate, and stability of the covalent phosphoenzyme was determined at various times by filtration on Whatman filters as described under "Materials and Methods."

lowed by 5 mM EGTA and 10 μM TG, remained completely stable over a week in the presence of decavanadate (*solid circles*). The long term stability of this species, however, appeared very sensitive to the residual concentration of free Ca^{2+}, showing slightly lower stability at 0.5 and 1.0 mM EGTA (Fig. 1*D*, *triangles* and *open circles*, respectively) than at 5 mM EGTA. This result is similar to the one previously found for phosphoenzyme formed from P_i, which is also stable in the presence of TG and decavanadate (18).

For optimal crystallization, we nevertheless observed that the EGTA concentration had to be lowered from 5 mM (used for producing the phosphoenzyme) to 0.5–1.0 mM. It is not clear why an elevated EGTA concentration inhibited crystallization; possibly, it was some direct effect of the polyanion on the crystallization process. In any case, crystallization appeared to be complete after overnight incubation on ice, at which time the preparations were fast frozen for electron microscopy. As indicated by our studies of phosphoenzyme stability under equivalent conditions, virtually no hydrolysis occurred over this time period (Fig. 1*D*), implying that essentially all ATPase molecules remained phosphorylated under the conditions of crystallization.

Structure of the FITC-labeled Phosphoenzyme—Images of thirteen tubular crystals were selected for image processing and three-dimensional reconstruction using methods of helical image analysis (27). These images consistently showed optical diffraction to at least 15-Å resolution. Unlike earlier work, only crystals conforming to a single helical symmetry were used for Fourier-Bessel reconstruction, allowing us to average data from all the tubes in Fourier space. Based on the 2-fold symmetry phase residual, we judged the resolution of our data to extend to 7-Å resolution (Table I).

This reconstruction revealed that the overall shape of the FITC-labeled, phosphorylated Ca^{2+}-ATPase (Fig. 2*A*) is surprisingly similar to that previously seen for the E_2·VO_4 conformation of unlabeled, unphosphorylated Ca^{2+}-ATPase crystallized under similar conditions either in the presence of TG (Fig. 2*B*) or in its absence (31–33). Also shown in Fig. 2*C* is a structure for FITC-labeled Ca^{2+}-ATPase that was not phosphorylated prior to crystallization (15). A noticeable hole is visible

TABLE I
Statistics of helical reconstructions

		FITC-*E*P·VO_4·TG		E_2·VO_4·TG		FITC-E_2·VO4·TG
No. tubes		13		58		12
No. repeats		22		95		22
Resolution Å	Residual[a] (degrees)	Data included[b] %	Residual (degrees)	Data included %	Residual (degrees)	Data included %
40	2.36	100	1.14	96	1.39	99
30	3.94	100	1.71	96	2.60	97
20	9.80	96	4.32	91	9.45	94
14	21.59	89	14.52	89	21.26	87
10	29.63	82	23.85	85	30.00	83
9			31.34	83	34.60	78
8	32.50	77	34.00	80	35.68	77
7	33.40	76				
6			36.33	77		

[a] Phase residual of final data set compared to ideal 2-fold symmetry (*i.e.*, 0 or 180°).
[b] Percentage of data remaining after removing data with phase error with respect to 2-fold symmetry >65°.

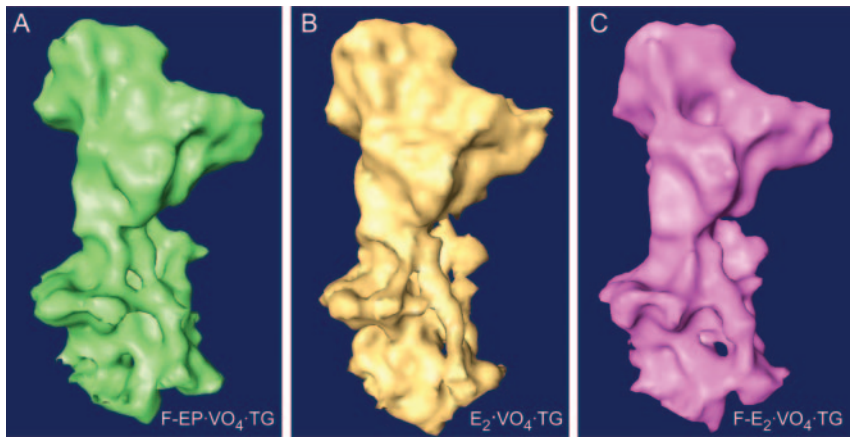

FIG. 2. **Three-dimensional reconstructions of the Ca^{2+}-ATPase in three different states.** The structure of the low fluorescence phosphoenzyme determined in the present work (*A*, F-EP·VO_4·TG) is shown together with structures of the native enzyme (*B*, E_2·VO_4·TG) and of the FITC-labeled, unphosphorylated enzyme (*C*, F-E_2·VO_4·TG), previously presented by Xu *et al.* (15). Crystallization conditions are the same in all three cases and include decavanadate and TG. Although at somewhat different resolutions (see Table I), all three structures have the same shape, suggesting that the domains have not significantly moved as a result of FITC labeling or phosphorylation. The only obvious difference is the hole in the middle of the cytoplasmic domain in F-E_2·VO_4·TG, which results from the exclusion of decavanadate from this site in this state.

in the cytoplasmic domain of the latter structure, which reflects the absence of decavanadate binding to this molecule (15), as will be further discussed below. TG was used for all the structures shown in Fig. 2, because it increases the abundance of tubular crystals present in the preparation; nevertheless, these crystals form in the absence of TG and we have previously shown that TG has no apparent effect on the disposition of the cytoplasmic domains (33).

We adopted two methods for comparing the FITC-labeled, phosphorylated Ca^{2+}-ATPase to the non-labeled, E_2·VO_4·TG form. First, we examined the detailed fit of an atomic model for Ca^{2+}-ATPase that was originally built for the E_2·VO_4·TG conformation (Fig. 3, pdb code 1KJU from Ref. 15). Using the program SITUS (34) to calculate a correlation coefficient for the fit, we found that this model fitted E_2·VO_4·TG and the present structure equally well (0.643 *versus* 0.649), thus precluding any significant domain displacements or significant reorganization of transmembrane helices. To look for more subtle differences between the two structures, we aligned the corresponding density maps in real space and calculated a difference map. All of the difference densities were found at the edges of the molecular envelope and probably reflect slight inaccuracies in alignment and differences in resolution between the two maps (Fig. 3*A*). Although some of these differences may indicate small structural changes, *e.g.* a small cavity within the phosphorylation domain of the FITC-labeled phosphoenzyme that was not observed in E_2·VO_4·TG, all of these are very much smaller than the obvious movements of cytoplasmic domains and transmembrane helices that characterize comparisons of E_2·VO_4·TG, $E_1(Ca_2)$, and E_2·TG (4). In comparison, a large, obvious negative difference density is visible in the control difference map between FITC-E_2·VO_4·TG and E_2·VO_4·TG (*red contours* in Fig. 3*B*), which results from the absence of decavanadate in the former structure (15). A similar set of difference densities was observed in comparing FITC-E_2·VO_4·TG with FITC-EP·VO_4·TG (data not shown). Thus, although FITC displaces decavanadate from its intramolecular binding site on unphosphorylated Ca^{2+}-ATPase, formation of the low fluorescence phosphoenzyme appears to reverse this effect. This difference in decavanadate binding to the phosphorylated and non-phosphorylated crystallized FITC-labeled ATPase must indicate a change in domain surfaces in this region of the molecule (see below).

Structural Insights from Glutaraldehyde Cross-linking and Proteolytic Digestion—Cross-linking the N- and P-domains of Ca^{2+}-ATPase by glutaraldehyde has been shown to be especially sensitive to the conformation of Ca^{2+}-ATPase. In particular, cross-linking of Lys^{492} in the N-domain to Arg^{678} in the P-domain is most efficient in the E_1P conformation and occurs with lower efficiency in $E_1(Ca_2)$ and E_2, whereas addition of either ATP or decavanadate to E_2, or formation of E_2-P, strongly inhibits cross-linking (35–37). In addition to showing these effects on control, unlabeled Ca^{2+}-ATPase samples, Fig. 4 shows results of glutaraldehyde cross-linking of FITC-labeled Ca^{2+}-ATPase, as detected by the appearance of a band migrat-

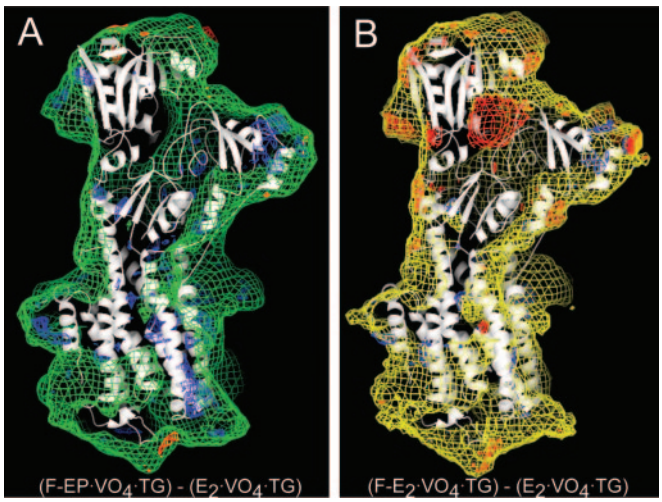

FIG. 3. **EM densities fitted with atomic coordinates and EM difference maps.** The *ribbon diagram* in *both panels* represents the pdb coordinates 1KJU that were previously fitted to the structure of E_2·VO_4·TG (15). Here, it is shown to fit equally well the density found for the unphosphorylated native E_2·VO_4·TG (*B*, *yellow envelope*) and the density found for the low fluorescence FITC-labeled phosphoenzyme F-EP·VO_4·TG (*A*, *green envelope*). Superposed with these densities, difference maps are also shown, as indicated: (F-EP·VO_4·TG − E_2·VO_4·TG) in *panel A*, for FITC-labeled phosphoenzyme relative to unphosphorylated unlabeled Ca^{2+}-ATPase, and (F-E_2·VO_4·TG − E_2·VO_4·TG) in *panel B*, for unphosphorylated FITC-labeled Ca^{2+}-ATPase relative to unphosphorylated unlabeled Ca^{2+}-ATPase. In *both panels*, the *blue* and *red* surfaces correspond to positive and negative difference densities, respectively, at a level of 5σ. A difference map between FITC-labeled phosphoenzyme and FITC-labeled unphosphorylated enzyme (F-E_2·VO_4·TG − F-EP·VO_4·TG) looks essentially the same as *panel B* (not shown): the only significant difference occurs at the intramolecular decavanadate site.

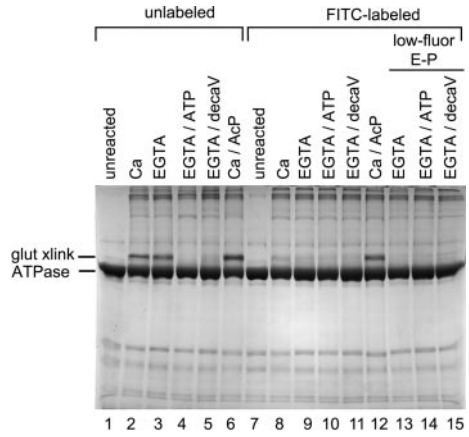

FIG. 4. **Cross-linking with glutaraldehyde.** SR vesicles were prepared in the native unlabeled state, labeled with FITC, or as the low fluorescence phosphoenzyme, as indicated. These vesicles were suspended at 0.4 mg/ml in a medium defined under "Materials and Methods," were reacted with glutaraldehyde (1 mM) for 4 min and then were subjected to SDS-PAGE followed by Coomassie Blue staining. Additional reagents added during the reaction are indicated at the top of each lane with concentrations as follows: 0.1 mM $CaCl_2$, 5 mM EGTA, 0.02 mM ATP, 0.04 mM decavanadate. The formation of a cross-link between Lys^{492} in N-domain and Arg^{678} in P-domain results in the formation of a species with an apparent molecular mass of 125 kDa as marked to the *left* of the gel.

ing at 125 kDa. In general, cross-linking is less efficient after labeling with FITC, but some general conclusions can still be drawn. Cross-linking occurs with lower efficiency for $E_1(Ca_2)$ (*lanes 2* and *8*) and E_2 (*lanes 3* and *9*). Although ATP strongly inhibits cross-linking of unlabeled Ca^{2+}-ATPase (*lane 4*), ATP cannot bind to FITC-labeled Ca^{2+}-ATPase and therefore has no effect on cross-linking (*lane 10*). In contrast, cross-linking of the E_1~P species formed at steady-state levels by AcP was almost equally efficient with labeled and unlabeled Ca^{2+}-ATPase (*lanes 6* and *12*, respectively); for FITC-labeled Ca^{2+}-ATPase, this steady-state species corresponds to the intermediate levels of fluorescence shown in Fig. 1*A*. However, formation of the low fluorescent phosphoenzyme from this steady-state E_1~P species produced very low cross-linking levels (*lane 13*), suggesting that the low fluorescence species no longer resembles E_1~P, from the point of view of glutaraldehyde cross-linking.

Proteolytic cleavage is another classic method for distinguishing conformations of Ca^{2+}-ATPase. We first considered digestion with proteinase K, which has a pair of diagnostic cleavage sites on the segments connecting M2 and M3 to the A domain (38). The latter site (Thr^{242}-E_2^{43}) represents the dominant cleavage site in the $E_1(Ca_2)$ conformation, thus producing the p83C fragment, whereas the former site (Leu^{119}-Lys^{120}) is specifically cleaved in E_2 and produces the p95C fragment in addition to the p83C fragment, particularly after binding of TG (Fig. 1 and Supplemental Material from Ref. 39). PK cleavage is dramatically reduced upon addition of nucleotide in the presence of Ca^{2+} ($E_1(Ca_2)$·ATP), upon formation of E_1P-like conformations, E_2-P, or E_2-P-like species formed with orthovanadate or decavanadate in the absence of Ca^{2+} (E_2·decaV) (40, 41). Here, we treated FITC-labeled Ca^{2+}-ATPase with PK after either inducing the low fluorescence phosphoenzyme (Fig. 5*A*, *lanes 5–8*), or stabilizing the E_2 conformation (Fig. 5*A*, *lanes 1–4*). AcP, EGTA, and TG were added in both cases, although EGTA was added *after* AcP to generate the phosphoenzyme but *before* AcP to simply stabilize an E_2 species. The resulting proteolytic patterns were indistinguishable, with both species creating a large amount of the p95C fragment, as is characteristic of E_2·TG. We therefore conclude that even though the low fluorescence phosphoenzyme is derived from the high energy phosphoenzyme, it resembles neither a normal E_1~P conformation nor an E_1 conformation, from the point of view of susceptibility to PK.

We finally turned to digestion with trypsin. Trypsin initially cleaves Ca^{2+}-ATPase at Arg^{505} to produce A and B fragments, which are not separated in our gel system, and fragment A is then cleaved at the T2 site to produce A1 and A2 subfragments. For native Ca^{2+}-ATPase, the susceptibility of the T2 site, which is at Arg^{198} on a loop not far from the conserved ^{181}TGES^{184} motif, is most sensitive to conformation (40–42). $E_1(Ca_2)$ is most susceptible to cleavage at T2, whereas formation of an E_2·vanadate complex in the absence of Ca^{2+} (using either orthovanadate or decavanadate, and presumably resembling E_2-P) completely blocks cleavage (40). Nucleotide binding to $E_1(Ca_2)$ or formation of the $E_1(Ca_2)$·AlF_4^- complex (presumably resembling E_1~P[Ca_2]) also protects the T2 site, but to a much lesser degree (41). Thus states analogous to E_2-P are distinguished by their resistance to cleavage at T2 with the remaining states showing relatively subtle differences. Fig. 5*B* shows that the tryptic digestion patterns of FITC-labeled Ca^{2+}-ATPase was also sensitive to the ligands present. *Lanes 1–6* show that the susceptibility of the T2 site after FITC labeling was similar to that of the native enzyme, *i.e.* most susceptible in the $E_1(Ca_2)$ (*lane 2*) and completely blocked in the presence of TG and either decavanadate or orthovanadate (*lanes 5* and *6*; it is however unclear whether decavanadate *per se* was responsible for this, or whether contaminating orthovanadate in the decavanadate solution was the active species). In the phosphorylated, low fluorescence species (*lane 7*), the T2 site remained highly susceptible to cleavage. However, in the presence of decavanadate (*lane 8*), the T2 site was blocked completely, almost as efficiently as in the non-phosphorylated E_2-type decavanadate complex. This suggests that the low fluorescence

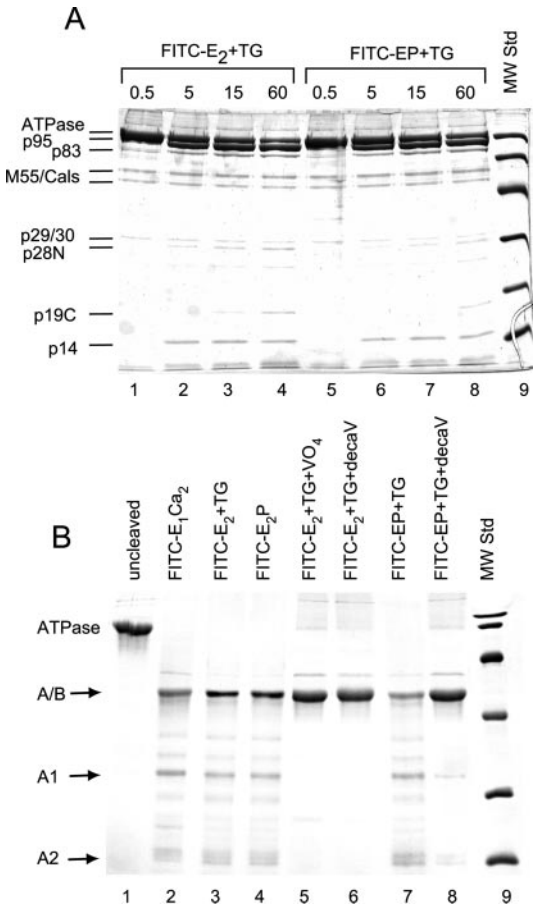

FIG. 5. **Digestion of FITC-labeled Ca^{2+}-ATPase with proteinase K (*A*) or trypsin (*B*).** *A*, for PK digestion, 2 mg/ml FITC-SR protein was suspended in 100 mM MOPS-NaOH, 5 mM Mg^{2+}, and 0.1 mM Ca^{2+}, at pH 6.5 and 20 °C. For *lanes 1–4*, 10 mM EGTA, 0.02 mg/ml TG, and 10 mM AcP were added sequentially, resulting in a control, high fluorescence, E_2-like state. For *lanes 5–9*, 10 mM AcP was added, followed first by 10 mM EGTA after 2 min, and then by 0.02 mg/ml TG, to form the stable low fluorescence phosphorylated species. Then, samples were digested with 0.03 mg/ml PK for the time intervals indicated at the *top* of each lane (minutes). The low fluorescence state was stable for at least 20 min after protease addition. *B*, for trypsin digestion, 0.75 mg/ml FITC-SR was suspended in 50 mM MOPS-NaOH, 0.1 mM Ca^{2+}, 5 mM Mg^{2+}, and 20% glycerol at pH 6.6 and 20 °C. For *lanes 3–6*, 5 mM EGTA was added; 10 μM TG (*lane 3*), 10 mM P_i (*lane 4*), 10 μM TG and 0.01 mM orthovanadate (*lane 5*), or 10 μM TG and 1 mM decavanadate (*lane 6*) were also added to produce the indicated intermediates. The low fluorescence phosphoenzyme (FITC-EP, *lanes 7–8*) was generated by adding 10 mM AcP followed after 2 min by 5 mM EGTA, and after another 30 s by 10 μM TG (*lane 7*) or 10 μM TG and 1 mM decavanadate (*lane 8*). For all samples, digestion was carried out with 0.015 mg/ml trypsin (ratio of 1/50 w/w) for 1 min. *Lane 9* shows molecular mass standards.

species is not a rigidly defined conformation but is still influenced by the binding of certain ligands and especially by decavanadate under the conditions used for crystallization.

DISCUSSION

Previous work reported conditions for forming a stable, phosphorylated form of Ca^{2+}-ATPase: after labeling with FITC, the enzyme is allowed to generate a steady-state Ca^{2+} gradient by cycling with AcP and is then treated with EGTA and TG to form an ultrastable, low fluorescence phosphoenzyme (Fig. 1). This low fluorescence phosphoenzyme is characterized by a high energy phosphoryl group in the sense that the protein is poised to transport Ca^{2+} as soon as Ca^{2+} binds to the cytoplasmically oriented, high affinity transport sites (16). Furthermore, this species is distinct from E_2-P, which either binds luminal Ca^{2+} with low affinity or, in the absence of luminal Ca^{2+}, is readily hydrolyzed into the unphosphorylated E_2 species. Thus, we had reasonable expectation that the FITC-labeled, low fluorescence phosphoenzyme would represent a good analogue for the E_1~P conformation. In the current work, we used [^{32}P] to document the stability of this phosphoenzyme under conditions of two-dimensional crystallization (Fig. 1) and reconstructed the three-dimensional structure at 8-Å resolution by cryoelectron microscopy (Fig. 2). Although this resolution is not sufficient to reveal atomic details, it does document the juxtaposition of cytoplasmic domains and the organization of transmembrane helices. Unexpectedly, we found that the conformation of the crystallized low fluorescence phosphoenzyme was in fact indistinguishable, at this resolution, from that of the native enzyme crystallized under equivalent conditions (Fig. 3). We then also used glutaraldehyde cross-linking and proteolysis as independent means of assessing the conformation of the low fluorescence species, and of potentially shedding light on the effect of decavanadate on its structure (Figs. 4 and 5). These studies suggested that the low fluorescence species was a hybrid, retaining characteristics of both Ca^{2+}-bound and Ca^{2+}-free species, and that its conformation was sensitive to the binding of decavanadate to the cytoplasmic domains.

Conformational Effects of FITC—The very low fluorescence of the species used for crystallization has previously been attributed either to an increase in pK_a of the phenolic 3-OH of fluorescein through hydrophobic/negatively charged interactions or to a salt link with basic residues surrounding the ATP pocket. Such interactions lead to a drastically stabilized aspartyl phosphate, presumably due to enhanced association of N- and P-domains (16). In particular, intimate communication between N- and P-domains would explain the interdependence of phosphoenzyme stability (in the P-domain) and fluorescein fluorescence (in the N-domain). The ATP binding pocket from the x-ray structure of E_1·ADP·AlF_4^- is shown in Fig. 6*A* with fluorescein substituted for ADP. Arg^{489}, Lys^{492}, Arg^{560}, and Arg^{678} are all nearby and represent potential ligands to clamp the phenolic residues at the ends of the xanthenolone ring of fluorescein (43), and stacking against the nearby Phe^{487} represents another potential stabilizing element (44). Specific interaction with these charged and/or aromatic side chains may account for fluorescent quenching after formation of E_1P. Arg^{678} is normally cross-linked to Lys^{492} by glutaraldehyde, especially in E_1P-like structures, and these residues are very close indeed in the E_1·ADP·AlF_4^- structure (Fig. 6*A*). In the E_2·VO_4·TG structure (Fig. 6*B*), the α-carbons for these residues have moved 13 Å further apart, which is consistent with the poor efficiency of cross-linking in E_2P-like reaction intermediates (35–37). According to our model, Arg^{678} is within range to interact with fluorescein in both conformations, which is a likely explanation for the inhibition of glutaraldehyde cross-linking after FITC labeling and after formation of the low fluorescence phosphoenzyme (Fig. 4). If so, FITC would be serving as a physical link between N- and P-domains, which may account for the extreme stability of the aspartyl phosphate in the low fluorescence state by perhaps altering the arrangement of catalytic residues in the phosphorylated P-domain, as well as restricting access of the A-domain to the catalytic site. Normally, phosphorylation induces a characteristic conformational change in the P-domain that allows its key residues to be gathered at the catalytic site. Additionally, the conserved ^{181}TGES^{184} sequence in the A-domain is able to approach the catalytic site in E_2-P and has been shown to have a critical role in orienting water for hydrolysis of the phosphoenzyme following Ca^{2+} release to the lumen (13, 39, 45). More generally, structural comparison of several Ca^{2+}-ATPase conformations indicates that the A-domain is highly mobile and undergoes

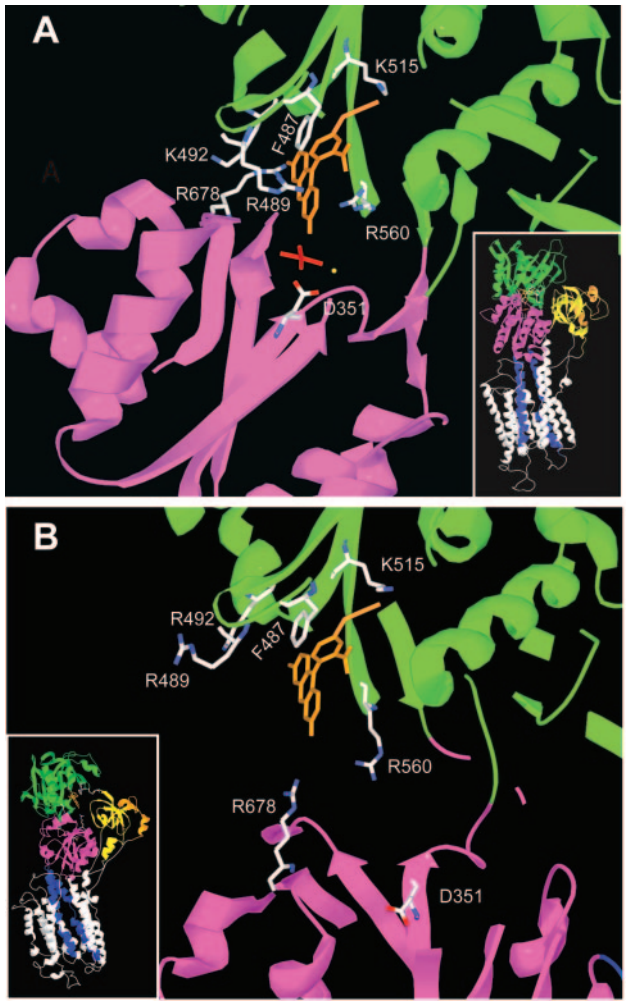

FIG. 6. **Model for the fluorescein binding site.** *A*, FITC (in *orange*) was placed into the ADP binding site of the x-ray structure for E_1·ADP·AlF_4^- (pdb code 1T5T) such that one 3-*O* phenolic oxygen superimposed with the β-phosphate of ADP and the isothiocyanate group on the benzoate ring was within binding range of Lys^{515}. This speculative model for the E_1·FITC·AlF_4^- species shows positively charged residues surrounding the xanthenolone ring of FITC, and the in-line disposition of its phenolic oxygen with AlF_4 (*red*); the position of one of the Mg^{2+} ions is also shown (*yellow*). Arg^{678} is in close proximity to Lys^{492}, which is consistent with the high efficiency of glutaraldehyde cross-linking observed for the E_1~P intermediate. *B*, an equivalent view of the E_2·FITC·VO_4·TG structure modeled from the cryoelectron microscopy (pdb code 1KJU), in which FITC occupies the same position within the N-domain. In the 1KJU structure, the P-domain (*magenta*) is pulled away from the N-domain (*green*) producing a large distance between FITC and Asp^{351}. Also, the α-carbon for Arg^{678} is 13 Å further away from Lys^{492}, accounting for the low efficiency of glutaraldehyde cross-linking in E_2P-like species. Nevertheless, the 3-*O* phenolic group of FITC is still within range for interaction with Arg^{678}. All views represent a 17-Å-thick slab at the interface of the N- and P-domains. *Insets* provide an overview of the entire molecule with the N-, P-, and A-domains shown in *green*, *magenta*, and *yellow*, respectively; M4 and M5 are colored *blue*, and other transmembrane helices are *white*. The figure was prepared with Swiss PDB Viewer and PovRay.

large rotations during the binding of Ca^{2+} to transport sites or during formation of the phosphoenzyme, thus allowing the ^{181}TGES^{184} loop to move from a solvent-exposed position in E_1 conformations to a buried position within the catalytic pocket in E_2-P (4, 13). Similarly, there is evidence that the N-domain is mobile in the $E_1(Ca_2)$ state (46) but becomes tethered to the P-domain during phosphate transfer from ATP, which elicits Ca^{2+} occlusion (12, 47). Although the FITC-labeled Ca^{2+}-ATPase is apparently still able to undergo all these steps and transport Ca^{2+}, the kinetics of Ca^{2+} occlusion appear to be altered, presumably due to the formation of a long-lived reaction intermediate immediately preceding closure of the cytoplasmic gates, which could be attributed to the persistence of the N/P-domain interface at the point in the cycle when ADP would normally be released (16).

Conformational Effects of Decavanadate—Decavanadate is required for two-dimensional crystallization of all three forms of Ca^{2+}-ATPase shown in Fig. 2: native Ca^{2+}-ATPase, FITC-labeled unphosphorylated Ca^{2+}-ATPase, and the low fluorescence phosphorylated species first studied here. Decavanadate has been shown to bind at two sites in the two-dimensional crystals of native Ca^{2+}-ATPase: one site mediating *inter*molecular contacts at a 2-fold symmetry axis and a second *intra*molecular site at the interface between N-, P-, and A-domains (48). Normally, FITC labeling completely displaces decavanadate from the intramolecular site (Fig. 2*C*) (15), a result consistent with a lowered binding stoichiometry for decavanadate measured under analogous conditions (49). Nevertheless, in the structure of the low fluorescence phosphoenzyme (FITC-EP·VO_4, Fig. 2*A*), density for decavanadate was clearly observed. This result must reflect some subtle alteration in the N-, P-, and A-domain interfaces upon formation of the low fluorescence state. Although the basis for binding the negatively charged decavanadate molecule ($V_{10}O_{29}^{6-}$) is uncertain, an atomic model for the unlabeled enzyme crystallized with decavanadate (pdb code 1KJU) shows positively charged residues from all three cytoplasmic domains surrounding the binding pocket, namely Arg^{489}, Lys^{492}, and Arg^{560} from the N-domain, Arg^{678} from the P-domain and Arg^{174} from the A-domain. Lys^{515} and Lys^{205} are also in the vicinity and could provide additional ligands depending on the orientation of their side chains. As previously mentioned, several of these residues may also interact with FITC; Arg^{489}, Lys^{492}, and Arg^{678} have also been specifically implicated in ATP ligation (37, 50) and Arg^{489} and Arg^{678} interact with AMPPCP and ADP in the relevant structures (12, 47). Thus, competition for these ligands could explain the competitive binding of decavanadate, ATP, and FITC to the unphosphorylated Ca^{2+}-ATPase as shown, for example, by the displacement of TNP-AMP by decavanadate (51).

Upon phosphorylation and formation of the low fluorescence species, these ligands and their corresponding domains appear to accommodate the binding of decavanadate, producing small but distinct fluorescence changes (Fig. 1), reducing the accessibility of the T2 proteolytic site (Fig. 5), and inducing crystallization. In fact, decavanadate probably further stabilizes the N-/P-domain interface. It is conceivable that in the low fluorescence phosphoenzyme, FITC no longer prevents decavanadate from binding at the intramolecular site, because specific interaction of FITC with one of the residues at this domain interface holds FITC in a favorable position. Protection of the T2 site of FITC-EP by decavanadate is consistent with rotation of the A-domain to the position seen in our new structure, which is indistinguishable from the position adopted by the unlabeled enzyme or by FITC-labeled, unphosphorylated enzyme (Figs. 2 and 3). Yet, the fact that the cytoplasmic domains adopt the same configuration in FITC-labeled unphosphorylated enzyme (F-E_2·VO_4·TG in Fig. 2), despite the lack of decavanadate binding, indicates that decavanadate is not stabilizing an artificial structure. In this respect, it is also notable that the 1KJU structure, which was fitted into the EM density derived from two-dimensional crystals of E_2·VO_4·TG, does not show any significant reorganization of cytosolic domains, compared with the structure of a decavanadate-free E_2P-like species recently derived from three-dimensional crystals of E_2·MgF_4·TG (47). Furthermore, although decavanadate does cause a small decrease

in fluorescence, probably due to Förster transfer, it does not fundamentally disrupt the low fluorescence state or the chemical stability of the aspartyl phosphate (18).

What Does Proteolysis Tell Us About the Structure?—Our tryptic digestion experiments suggest that, prior to the addition of decavanadate, the low fluorescence species has a relatively exposed T2 cleavage site, perhaps similar to E_1. However, the pattern of PK digestion most closely resembles that of E_2. The T2 site (Arg^{198}) is on a loop in the mobile A-domain, which is held firmly against the P-domain in $E_2{\cdot}VO_4$ or is rotated by 90° in $E_1(Ca_2)$ and thus exposed to solvent. Similarly, the PK site ($Leu\text{-}Lys^{120}$) is on the link between the A-domain and transmembrane helix M2, and its susceptibility is influenced by interaction of the M2 and M3 links with the P-domain (39). The hybrid behavior of the low fluorescence species might reflect structural flexibility arising 1) from the lack of Ca^{2+} at the transport sites and 2) from the inability to form a true E_2-P structure at the catalytic site. Such flexibility was previously invoked to explain the fact that $E_1(Ca_2){\cdot}$AMPPCP is considerably more susceptible to PK than $E_1(Ca_2){\cdot}ADP{\cdot}AlF_4^-$, despite having virtually identical atomic structures; in this case, the susceptibility to PK also correlated with inability to occlude Ca^{2+} (12). In the case of our low fluorescence species, flexibility of its A-domain is consistent with the effectiveness of either orthovanadate or decavanadate in inhibiting tryptic cleavage at the T2 site and in stabilizing the A-domain in the position seen in our structure. PK proteolytic patterns for the low fluorescence phosphoenzyme are indistinguishable from those for the unphosphorylated enzyme in the absence of Ca^{2+} and in the presence of TG (with or without FITC), which is consistent with the ability of vanadate to induce similar structures for all three forms (Fig. 2). We conclude that the conformation of the low fluorescence phosphoenzyme is significantly influenced by the various ligands studied, *i.e.* orthovanadate or decavanadate, and of course Ca^{2+}, as it binds to transport sites and induces the enzyme to reenter the catalytic cycle.

Ca^{2+} Is a Dominant Determinant of Ca^{2+}-ATPase Conformation—X-ray structures show that Ca^{2+} has a profound effect on the transmembrane helices, causing curving of the central M5 helix and large displacements of M1, M2, M3, M4, and M6. These changes are presumably initiated by recruitment of ligands to bind the pair of Ca^{2+} ions and relaxation of these same ligands into a significantly different configuration in the absence of Ca^{2+}. In contrast, these structures show that the presence of ligands at the catalytic site have relatively minor effects on the structure of the membrane helices (*e.g.* compare $E_2{\cdot}$TG and $E_2{\cdot}MgF_4{\cdot}$TG in Ref. 13, and compare $E_1(Ca_2)$ and $E_1{\cdot}$AMPPCP in Ref. 47). These observations are in line with the fact that TG binds only to Ca^{2+}-free, E_2-like species of Ca^{2+}-ATPase (52, 53), and the ability of TG to stabilize the FITC-labeled, low fluorescence species suggests that in this species the transmembrane helices adopt an E_2-like configuration, which is likely to be a direct result of Ca^{2+} dissociation from the FITC-labeled E_1P species present at steady state. Indeed, the membrane domain in our current structure of the low fluorescence phosphoenzyme is identical to that of $E_2{\cdot}VO_4$, at least at 6- to 7-Å resolution, and certainly distinct from the structure expected for an E_1 conformation. The lesson would seem to be that Ca^{2+} is the primary determinant of the global conformation of Ca^{2+}-ATPase, given its definitive influence over the entire transmembrane domain and its ability to control cytoplasmic domain associations and thus ligand binding. Obviously, the cytoplasmic domains are also able to exert some influence over the membrane domain, but this appears to be confined to relatively minor structural changes that open and close gates that control access of Ca^{2+} to the binding sites, as well as to some as yet undefined mechanism of altering Ca^{2+} affinity during the $E_1{\sim}P[Ca_2]$ to E_2-P[Ca] transition.

An Alternative Hypothesis: Phosphotransfer to Fluorescein—A completely different explanation for the stability of the phosphoenzyme could be that Ca^{2+} removal from the FITC-labeled species formed from AcP at steady state (with intermediate fluorescence) elicits unexpected phosphate transfer from Asp^{351} to a phenolic oxygen of the covalently attached fluorescein. Because the pH sensitivity of the spectral properties of fluorescein is due to protonation or deprotonation of one of the phenolic oxygens, covalent attachment of phosphate at the same site on fluorescein would no doubt also alter its spectral properties: phosphorylation of fluorescein is already known to result in low fluorescence (54), and 3-methylfluorescein monophosphate is a commonly used non-fluorescent but fluorogenic substrate for phosphatases as well as for Ca^{2+}-ATPase (55). Furthermore, phosphate transfer from Asp^{351} to FITC would provide an elegant explanation for our findings that high fluorescence and low fluorescence forms of FITC-ATPase have similar proteolytic patterns and cross-linking properties. Indeed, the model of fluorescein docked in the structure of $E_1{\cdot}ADP{\cdot}AlF_4^-$ (Fig. 6*A*) shows that the 3-*O* of the xanthenolone ring can be superimposed with the terminal oxygen of the β-phosphate, which is in line with the γ-phosphate analog AlF_4^-. Upon removal of Ca^{2+}, Arg^{678} might thus provide an alternative interaction for the covalently attached fluorescein monophosphate. After re-addition of Ca^{2+}, the attached fluorescein monophosphate could act as a substrate for re-phosphorylation of Asp^{351}, thus allowing Ca^{2+}-ATPase to re-enter the catalytic cycle. There is a precedent for such a mechanism: TNP-ATP covalently attached to Lys^{492} through a light-dependent azido reaction is capable of serving as a substrate upon the addition of Ca^{2+} (56). We investigated this possibility by analyzing tryptic digests of FITC-labeled Ca^{2+}-ATPase prepared from control and low fluorescent phosphoenzyme preparations. The two main fluorescein-peptides were found to have indistinguishable retention times on C18 reverse-phase high performance liquid chromatography and virtually identical absorption spectra, as characterized by the optical density ratio at 210 and 495 nm (data not shown). Furthermore, the pH dependence of absorbance in 8 M urea of the covalently attached fluorescein was similar whether it was derived from control or from the low fluorescence species, which in turn was like that of FITC itself: pK_a values were close to 7, and were quite different from the pK_a of 4.9 for fluorescein monophosphate in solution (54) (data not shown). Based on these results, phosphate transfer from Asp^{351} to the fluorescein ring does not appear to be the most likely explanation for the appearance of our low fluorescence species; rather, we attribute the low fluorescence to a unique interaction between N- and P-domains that serves to protect the aspartyl phosphate bond. However, covalent binding to Ca^{2+}-ATPase of the putative fluorescein monophosphate could well modify its properties in unexpected ways, and the alternative hypothesis should perhaps be kept in mind.

Acknowledgments—We thank F. Henao for his help with some of the fluorescence measurements and G. Lenoir for his help with some of the SDS-PAGE experiments, J. C. Robert for his help with covalent phosphoenzyme and SDS-PAGE experiments, and J. Navaza for his help with comparison of the EM structure using the program URO.

REFERENCES

1. Fagan, M. J., and Saier, M. H. (1994) *J. Mol. Evol.* **38,** 57–99
2. Lutsenko, S., and Kaplan, J. H. (1995) *Biochemistry* **34,** 15607–15613
3. Mintz, E., and Guillain, F. (1997) *Biochim. Biophys. Acta* **1318,** 52–70
4. Stokes, D. L., and Green, N. M. (2003) *Annu. Rev. Biophys. Biomol. Struct.* **32,** 445–468
5. Toyoshima, C., and Inesi, G. (2004) *Annu. Rev. Biochem.* **73,** 269–292

6. Jencks, W. P. (1989) *J. Biol. Chem.* **264,** 18855–18858
7. Kuhlbrandt, W. (2004) *Nat. Rev. Mol. Cell. Biol.* **5,** 282–295
8. Toyoshima, C., Nakasako, M., Nomura, H., and Ogawa, H. (2000) *Nature* **405,** 647–655
9. Toyoshima, C., and Nomura, H. (2002) *Nature* **418,** 605–611
10. DeJesus, F., Girardet, J. L., and Dupont, Y. (1993) *FEBS Lett.* **332,** 229–232
11. Chen, Z., Stokes, D. L., Rice, W. J., and Jones, L. R. (2003) *J. Biol. Chem.* **278,** 48348–48356
12. Sorensen, T. L., Møller, J. V., and Nissen, P. (2004) *Science* **304,** 1672–1675
13. Toyoshima, C., Nomura, H., and Tsuda, T. (2004) *Nature* **432,** 361–368
14. Olesen, C., Sorensen, T. L., Nielsen, R. C., Moller, J. V., and Nissen, P. (2004) *Science* **306,** 2251–2255
15. Xu, C., Rice, W. J., He, W., and Stokes, D. L. (2002) *J. Mol. Biol.* **316,** 201–211
16. Champeil, P., Henao, F., Lacapere, J. J., and McIntosh, D. B. (2001) *J. Biol. Chem.* **276,** 5795–5803
17. Pick, U., and Karlish, S. J. D. (1980) *Biochim. Biophys. Acta* **626,** 255–261
18. Henao, F., Delavoie, F., Lacapere, J. J., McIntosh, D. B., and Champeil, P. (2001) *J. Biol. Chem.* **276,** 24284–24285
19. Delavoie, F., McIntosh, D., Henao, F., Peranzi, G., Champeil, P., Stokes, D., and Lacapere, J. J. (2003) *Ann. N. Y. Acad. Sci.* **986,** 17–19
20. Delavoie, F., Peranzi, G., Maccario, J., and Lacapere, J. J. (2001) *Biol. Cell* **93,** 363–366
21. Eletr, S., and Inesi, G. (1972) *Biochim. Biophys. Acta* **282,** 174–179
22. Champeil, P., Guillain, F., Venien, C., and Gingold, M. P. (1985) *Biochemistry* **24,** 69–81
23. Warren, G. B., Toon, P. A., Birdsall, N. J. M., Lee, A. G., and Metcalfe, J. C. (1974) *Proc. Natl. Acad. Sci. U. S. A.* **71,** 622–626
24. Bodley, A. L., and Jencks, W. P. (1987) *J. Biol. Chem.* **262,** 13997–14004
25. Møller, J. V., Lenoir, G., Marchand, C., Montigny, C., le Maire, M., Toyoshima, C., Juul, B. S., and Champeil, P. (2002) *J. Biol. Chem.* **277,** 38647–38659
26. Tani, K., Sasabe, H., and Toyoshima, C. (1996) *Ultramicroscopy* **65,** 31–44
27. Beroukhim, R., and Unwin, N. (1997) *Ultramicroscopy* **70,** 57–81
28. Frank, J., Radermacher, M., Penczek, P., Zhu, J., Li, Y., Ladjadj, M., and Leith, A. (1996) *J. Struct. Biol.* **116,** 190–199
29. Pick, U., and Bassilian, S. (1981) *FEBS Lett.* **123,** 127–130
30. Highsmith, S., Barker, D., and Scales, D. J. (1985) *Biochim. Biophys. Acta* **817,** 123–133
31. Toyoshima, C., Sasabe, H., and Stokes, D. L. (1993) *Nature* **362,** 469–471
32. Zhang, P., Toyoshima, C., Yonekura, K., Green, N. M., and Stokes, D. L. (1998) *Nature* **392,** 835–839
33. Young, H., Xu, C., Zhang, P., and Stokes, D. (2001) *J. Mol. Biol.* **308,** 231–240
34. Wriggers, W., Milligan, R. A., and McCammon, J. A. (1999) *J. Struct. Biol.* **125,** 185–195
35. Ross, D. C., and McIntosh, D. B. (1987) *J. Biol. Chem.* **262,** 2042–2049
36. Ross, D. C., Davidson, G. A., and McIntosh, D. B. (1991) *J. Biol. Chem.* **266,** 4613–4621
37. Mcintosh, D. B. (1992) *J. Biol. Chem.* **267,** 22328–22335
38. Juul, B., Turc, H., Durand, M. L., Gomez de Gracia, A., Denoroy, L., Moller, J. V., Champeil, P., and le Maire, M. (1995) *J. Biol. Chem.* **270,** 20123–20134
39. Lenoir, G., Picard, M., Gauron, C., Montigny, C., Le Marechal, P., Falson, P., Le Maire, M., Moller, J. V., and Champeil, P. (2004) *J. Biol. Chem.* **279,** 9156–9166
40. Danko, S., Daiho, T., Yamasaki, K., Kamidochi, M., Suzuki, H., and Toyoshima, C. (2001) *FEBS Lett.* **489,** 277–282
41. Danko, S., Yamasaki, K., Daiho, T., Suzuki, H., and Toyoshima, C. (2001) *FEBS Lett.* **505,** 129–135
42. Andersen, J. P., Vilsen, B., Collins, J. H., and Jorgensen, P. L. (1986) *J. Membr. Biol.* **93,** 85–92
43. Whitlow, M., Howard, A. J., Wood, J. F., Voss, E. W., Jr., and Hardman, K. D. (1995) *Protein Eng.* **8,** 749–761
44. Korndorfer, I. P., Beste, G., and Skerra, A. (2003) *Proteins* **53,** 121–129
45. Clausen, J. D., Vilsen, B., McIntosh, D. B., Einholm, A. P., and Andersen, J. P. (2004) *Proc. Natl. Acad. Sci. U. S. A.* **101,** 2776–2781
46. Huang, S., and Squier, T. C. (1998) *Biochemistry* **37,** 18064–18073
47. Toyoshima, C., and Mizutani, T. (2004) *Nature* **430,** 529–535
48. Stokes, D. L., and Green, N. M. (2000) *Biophys. J.* **78,** 1765–1776
49. Csermely, P., Varga, S., and Martonosi, A. (1985) *Eur. J. Biochem.* **150,** 455–460
50. McIntosh, D. B., Woolley, D. G., Vilsen, B., and Andersen, J. P. (1996) *J. Biol. Chem.* **271,** 25778–25789
51. Hua, S., Inesi, G., and Toyoshima, C. (2000) *J. Biol. Chem.* **275,** 30546–30550
52. Sagara, Y., Wade, J. B., and Inesi, G. (1992) *J. Biol. Chem.* **267,** 1286–1292
53. Seekoe, T., Peall, S., and McIntosh, D. B. (2001) *J. Biol. Chem.* **276,** 46737–46744
54. Huang, Z., Wang, Q., Ly, H. D., Gorvindarajan, A., Scheigetz, J., Zamboni, R., Desmarais, S., and Ramachandran, C. (1999) *J. Biomol. Screen.* **4,** 327–334
55. Everts, M. E., Andersen, J. P., Clausen, T., and Hansen, O. (1989) *Biochem. J.* **260,** 443–448
56. McIntosh, D. B., and Woolley, D. G. (1994) *J. Biol. Chem.* **269,** 21587–21595

Structural Studies of a Stabilized Phosphoenzyme Intermediate of Ca^{2+}-ATPase

David L. Stokes, Franck Delavoie, William J. Rice, Philippe Champeil, David B. McIntosh and Jean-Jacques Lacapère

J. Biol. Chem. 2005, 280:18063-18072.
doi: 10.1074/jbc.M500031200 originally published online February 25, 2005
